The role of excited electronic states in ambient air ionization by a nanosecond discharge

Nicolas Minesi, Pierre Mariotto, Erwan Pannier, Gabi D. Stancu, Christophe O Laux

The role of excited electronic states in ambient air ionization by a nanosecond discharge

N. Minesi, P. Mariotto, E. Pannier, G. D. Stancu and C. O. Laux

EM2C, CNRS, CentraleSupélec, Université Paris Saclay, 3 Rue Joliot-Curie, 91190 Gif-sur-Yvette, France

The mechanism of air ionization by a single nanosecond discharge under atmospheric conditions is studied using numerical simulations. The plasma kinetics are solved with ZDPlasKin and the electron energy distribution function is calculated with BOLSIG+. The model includes the excited electronic states of O and N atoms, which are shown to play the main role in plasma ionization for $n_e > 10^{16}$ cm^{-3}. For electric fields typical in nanosecond discharges, a non-equilibrium plasma ($T_e > T_{gas}$) is formed at ambient conditions and remains partially ionized for about 12 nanoseconds ($n_e < 10^{16}$ cm^{-3}). Then, the discharge abruptly reaches full ionization ($n_e \approx 10^{19}$ cm^{-3}) and thermalization ($T_e = T_{gas} \approx 3$ eV) in less than half a nanosecond, as also encountered in experimental studies. This fast ionization process is explained by the electron impact ionization of atomic excited states whereas the fast thermalization is induced by the elastic electron-ion collisions.

I. Introduction

Nanosecond Repetitively Pulsed (NRP) discharges usually produce weakly ionized, non-equilibrium plasmas in air [1–6]. The different states of non-equilibrium NRP plasmas (corona, glow, and spark) have been described by Pai *et al.* [2]. However, other works [7–14] have shown that nanosecond discharges can also produce fully ionized thermal plasmas. This type of nanosecond discharge, called the thermal spark, is in thermal equilibrium [7] and differs from the NRP spark described by Pai *et al.* [2]. Parkevich and co-authors showed by laser interferometry that, at atmospheric conditions, full ionization is reached first close to the electrodes [8,9]. In Ref. [12], Orriere *et al*. studied the formation of plasma during a 2.5-kV pulse of 10 ns in ambient air. The distance between the electrodes was 200 μm and the maximum reduced field E/N was 600 Td (1 Td = 10^{-17} V.cm^2). From the Stark

broadening of H, O, and N lines, Orriere *et al*. measured electron number densities reaching about 10^{19} cm^{-3}. Electron number densities higher than 10^{18} cm^{-3} were also measured in nanosecond Surface Dielectric Barrier Discharges (SDBD) [15–17]. The authors of Ref. [15–17] demonstrated that increasing the initial pressure induced a transition from a partially to a fully ionized SDBD. The role of the initial pressure increase was later confirmed experimentally in pin-to-pin configurations [7].

Simulations of partially ionized plasmas have already been performed [18,19] with the kinetic mechanism of Kossyi *et al.* [20] or Capitelli *et al.* [21] that are well suited for simulations of non-equilibrium plasmas. Shcherbanev *et al.* [16] proposed that the ionization of nanosecond discharges could be accelerated by the ionization of the N_2(B, C) states. They showed that the inclusion of these states in their chemical mechanism increased the ionization rate, but full ionization was not reached. A chemical kinetic model describing the complete mechanism of the thermal spark formation by a single nanosecond discharge in air is yet to be attempted.

The article is organized as follows. The kinetic mechanism is described in Section II, and details about the ionization and recombination rates are given in Section III. Then, in Section IV, the results of the simulation are provided and the mechanisms of ionization is described. In Section V, we demonstrate the impact of electron-ion elastic collisions on the gas temperature increase, and, in Section VI, we discuss the departure of the EEDF from a Maxwellian distribution. In Section VII, we show the influence of atomic excited states on the kinetics of thermal spark. In Section VIII, we simulate the kinetics of the thermal spark, assuming a constant electron temperature, instead of a given electric field. Finally, we conclude on the kinetics of the thermal spark. Additional details on the role of the ionization of N_2 excited states are discussed in the Appendix.

II. Kinetic mechanism

In the present study, numerical simulations of plasma kinetics under a fixed electric field are performed using ZDPlasKin [22]. The baseline kinetic mechanism is taken from the work of Capitelli *et al.* [21]. This reaction set has already been used to simulate non-equilibrium nanosecond discharges with

$T_{gas} \ll T_e$ [23] and is available online[1]. In this work, the Electron Energy Distribution Function (EEDF) is calculated, solving the Boltzmann equation with BOLSIG+ [24,25]. The cross-sections of electron reactions are taken mostly from the LXCat database [26–29]. The primary cross-sections we use are taken from the *LXCat IST-Lisbon* database [27]. Concerning nitrogen, most of the cross-sections of Ref. [27] are taken from the *LXCat Phelps* database and extended to higher energies. The *LXCat Hayashi* database is used for the elastic et ionization cross-section of N_2O [28]. The *LXCat Morgan* database provides the electron impact cross-sections of O^- and O_3 [29]. The effects of dissociation, ionization, and super-elastic collisions are always considered in the EEDF calculation, whereas electron-electron collisions are included for an ionization fraction above 10^{-5}. The remaining BOLSIG+ parameters are kept on default [30]. Thus, after ionization by electron-impact, the remaining energy is shared equally and the EEDF is calculated assuming a purely temporal growth.

We supplement the baseline model with the ionization and dissociation of N_2 electronic states (X, A, B, C, and a') by electron impact (Reac. 1 and Reac. 2) because they can play a role in the ionization process [16,31].

$$N_2(\mathrm{X,A,B,C,a'}) + e \rightleftharpoons N_2^+(X,A,B,C) + e + e \qquad \text{Reac. 1}$$

$$N_2(\mathrm{X,A,B,C,a'}) + e \rightleftharpoons N(^4S,^2D) + N(^4S) + e \qquad \text{Reac. 2}$$

The excitation and dissociation by electron impact of N_2^+ electronic states (X, A, B, C) are also included [31].

The originality of the present model is to consider not only the excited electronic states of N_2 and N_2^+, but also the excited electronic states of O and N.

$$N(^4S,^2P,^2D,\dots) + e \rightleftharpoons N^+(^3P) + e + e \qquad \text{Reac. 3}$$

$$O(^3P,^1D,^1S) + e \rightleftharpoons O^+(^4S) + e + e \qquad \text{Reac. 4}$$

The model incorporates the first eight electronic levels of N, and the first three electronic levels of O. Only the ionization rates to the ground state of the ions, $N^+(^3P)$ and $O^+(^4S)$, are calculated because the

[1] www.zdplaskin.laplace.univ-tlse.fr/author/sergey-pancheshnyi/index.html

ionization to other states is negligible [32]. In all simulations performed in this work, the initial gas temperature is 300 K, and the initial electron temperature is 1000 K. The initial number density of the gas (79% N_2 and 21% O_2) is equal to $n_0 = 2.45\times10^{19}$ cm^{-3}. The initial electron number density is taken as $n_{e0} = 10^{10}$ cm^{-3} and the integration step is 2 ps. We found that increasing or decreasing the initial electron number density from 10^9 to 10^{11} cm^{-3} only shifts the kinetic curves in time by less than 1 ns.

In Section III to Section VII, a constant electric field is imposed up to 15 ns, after a voltage rise time of 2 ns. The simulation is stopped at t = 15 ns. The reduced electric field varies as given by Eq. 1, where E_0 is amplitude of the applied field.

$$\mathrm{E\ [V.cm^{-1}\ ]} = \begin{cases} E_0 \times \dfrac{t}{2\ \mathrm{ns}}, & t \leq 2\ \mathrm{ns} \\ E_0, & 2\ \mathrm{ns} \leq t \leq 15\ \mathrm{ns} \end{cases} \qquad \text{Eq. 1}$$

A field $E_0 = 47$ kV·cm^{-1} is applied which corresponds to $(E/N)_0 = 195$ Td in ambient conditions (T = 300 K, p = 1 atm). This generic pulse is representative of a 5-kV pulse applied across a 1-mm gap. In BOLSIG+, the reduced field E/N is the ratio of the electric field to the neutral particle density, $N_{neutral}$. As we will see in the present work, however, the neutral particle density can drop to negligible values, and the reduced field tends toward infinity. Thus, the electron temperature increases above reasonable values. Therefore, we define N as the heavy particle density, i.e. $N = N_{ion} + N_{neutral}$.

Another approach consists instead in imposing the electron temperature. Thus, in Section VIII, we simulated a nanosecond pulse with a constant electron temperature. The results obtained in Section VIII agree with those obtained in previous sections and show that both methods provide equivalent results.

III. Determination of ionization and recombination rates

In this section, the procedure to determine the ionization and recombination rate coefficients used in Reac. 1, Reac. 3, and Reac. 4 is detailed.

The ionization rate coefficients of Reac. 3 and Reac. 4 are calculated with BOLSIG+ using the ionization cross-sections of the first three levels of O and N calculated by the B-spline R-matrix (BSR) approach [32,33] (see Table 1). For states above N(^{2}D) and up to N(^{4}D^0), the ionization rate coefficients

of Ref. [34] are used. For N_2(X) ionization to N_2^+(X, B), the cross-sections are from the LXCat *LISBON database* [27], whereas the ionization cross-sections to N_2^+(A, C) are taken from the work of Bacri and Medani [31]. The ionization cross-sections of N_2(A, B, C, a') are taken from Ref. [31]. The electron-impact ionization of N^+ and O^+ to N^{++} and O^{++} is also considered in Section VIII, using the cross-sections compiled in Ref. [35]. These later processes are found to have a minor impact under the present conditions.

Table 1 Electronic levels of N and O included in the present work. The excitation rate coefficients between states are computed with BOLSIG+ at every time step based on the BSR cross-sections calculated in Ref. [32,33]**. When available, the ionization BSR cross-sections are used; otherwise, the reaction rates computed in Ref.** [34] **based on BEB cross-sections are used. All reverse rates are calculated by detailed balancing.**

State	Configuration	g	E_{up} (eV)	Electronic transitions rate	Ionization rate
$N(^4D^0)$	$2s^22p^2(^3P)3p$	20	11.75	Integral of BSR cross-section [32]	Arrhenius rate [34]
$N(^2S^0)$	$2s^22p^2(^3P)3p$	2	11.60		
$N(^4P)$	$2s^22p^4$	12	10.92		
$N(^2P)$	$2s^22p^2(^3P)3s$	6	10.68		
$N(^4P)$	$2s^22p^2(^3P)3s$	12	10.33		
$N(^2P^0)$	$2s^22p^3$	6	3.575	Integral of BSR cross-section [32]	Integral of BSR cross-section [32]
$N(^2D^0)$	$2s^22p^3$	10	2.38		
$N(^4S^0)$	$2s^22p^3$	4	0		
$O(^1S)$	$2s^22p^4$	1	4.19	Integral of BSR cross-section [33]	
$O(^1D)$	$2s^22p^4$	5	1.97		
$O(^3P)$	$2s^22p^4$	9	0		

The three-body recombination rate coefficients of N^+ have been computed in various studies [36–41]. These global rate coefficients do not differentiate recombination into different electronic states of the atoms. A compilation of several recombination rates is shown in Fig. 1. A recombination coefficient rate valid for any given ion is calculated by Bibermann *et al.* [42]. This coefficient is proportional to $T_e^{-4.5}$ and said to be valid if T_e is smaller than the energy of the first excited state of the considered atom. Capitelli *et al.* [21] stated later that this rate is only valid below 2000 K. Bibermann *et al.* [42] also calculated the N^+ recombination rate coefficients at several temperatures (reported in Fig. 1). The deviation between the $T_e^{-4.5}$ law and the N^+ recombination rate coefficient begins at $T_e \sim 2000$ K, which

justifies the more restrictive limit defined by Capitelli *et al.* A review of N^+ and O^+ three-body recombination rates can be found in Ref. [39]. However, these rates will not be used because a state-specific model is employed.

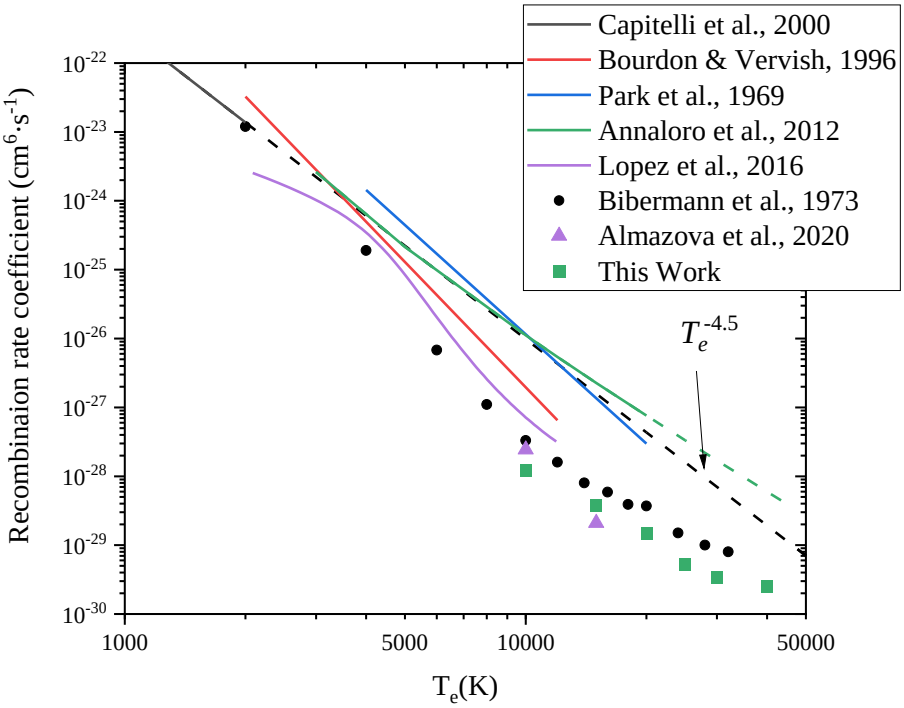

Fig. 1 Comparison of recombination rate coefficients of N^+ available in the literature [36–41]**. The rate coefficients reported by Capitelli *et al.* and Almazova *et al.* are for any ion, whereas the others are specific to N^+. In these references, $N^+(^3P)$ recombines into the atomic ground state $N(^4S)$. The solid lines indicate the validity range of the rate coefficients and the dashed lines correspond to extrapolations. The global recombination rates calculated with the present mechanism include only 8 electronic levels of N.**

In the present simulations, the state-specific recombination rates are computed by detailed balance (or Saha formula) [43,44] according to Eq. 2, where m_e is the electron mass, k_b the Boltzmann constant, T_e the electron temperature, h the Planck constant, g_A the degeneracy of level A_i, I_A the ionization energy of A relative to the ground state, E_{A_i} the energy of the electronic state A_i relative to the ground state, and $k_{f,i}$ the ionization rate.

$$k_{r,i} = \frac{1}{2}\left(\frac{2\pi m_e k_b T_e}{h^2}\right)^{-1.5} \frac{g_{A_i}}{g_{A^+}} \exp\left(\frac{\mathrm{I_A} - E_{A_i}}{k_b T_e}\right) k_{f,i} \qquad \text{Eq. 2}$$

Eq. 2 is strictly valid only if the EEDF is a Maxwellian. In Section VI, we show that the deviation of the EEDF from a Maxwellian has a negligible impact under our conditions. Therefore, the recombination rates of N^+ (O^+) to the first 8 (3) electronic levels of N (O) are calculated via detailed balance. These levels are listed in Table 1 and are all included in the kinetic mechanism unless otherwise specified. A representation of the states and reactions involved in the case of N is shown in Fig. 2. Using the present mechanism, a global recombination rate of N^+ is calculated and presented in Fig. 1. Our results are consistent with the literature. However, this global recombination rate strongly depends on the electronic states grouping and the ionization/excitation cross-sections [41]. In the present case, the electronic levels of N above 11.8 eV have been omitted, which could have an impact on the effective recombination rates presented in Fig. 1.

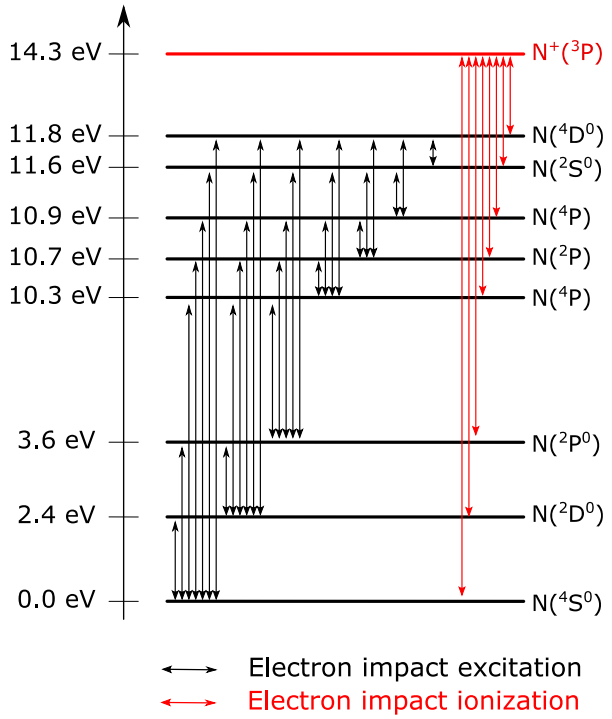

Fig. 2 Electronic transitions by electron impact (in black) and ionization by electron impact (in red) of atomic nitrogen. The reverse rates are calculated by detailed balance.

IV. Ionization mechanism

The reduced electric field is proportional to the applied external field, E, which is constant after 2 ns, and inversely proportional to the total gas number density, which eventually increases when N_2 and O_2 dissociate. The variations of E/N are shown in Fig. 3.

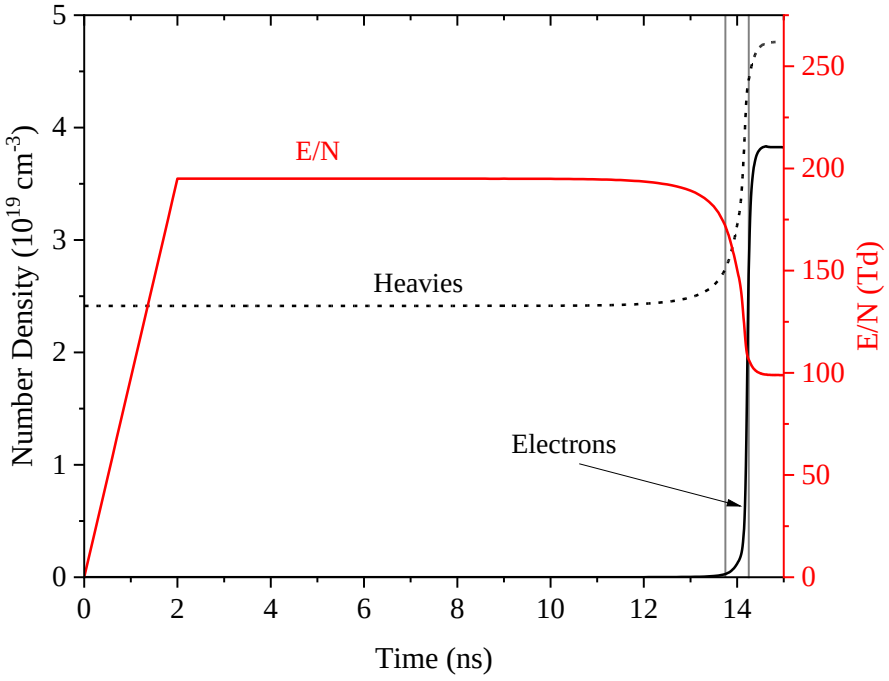

Fig. 3 Variation of the electron number density during the 15-ns pulse (solid black line). The decrease of the reduced electric field (solid red line) is due to the increase of the heavy particle density (dashed black line) owing to dissociation. The period of fast ionization is delimited by the grey lines between 13.75 and 14.25 ns.

For t < 12 ns, more than 95% of the electrical power is spent on inelastic collisions. At t = 12 ns, the reduced field begins to decay due to molecular dissociation. Between 13.75 and 14.25 ns, the atoms fully ionize, the electron number density gains two orders of magnitude, and the plasma transitions from a non-equilibrium to a thermalized plasma and. This result corresponds to earlier observations of fully ionized filaments, abruptly generated by nanosecond discharges in less than 0.5 ns [7,11,12]. During this short period, the fraction of power exchanged through elastic collisions reaches nearly 50%. At the end of the simulated pulse, the electron number density is $n_e \approx 4 \cdot 10^{19}$ cm^{-3}. The power exchanged through elastic collisions is null because T_{gas} is equal to T_e. For t > 15 ns, the plasma enters an isentropic expansion phase (until at least t = 100 ns) [7,11] that is not modeled here. The main plasma parameters

during the transition are given in Table 2 and the evolution of the number densities of N_2, O_2, N, O, N^+, and O^+ is given in Fig. 4.

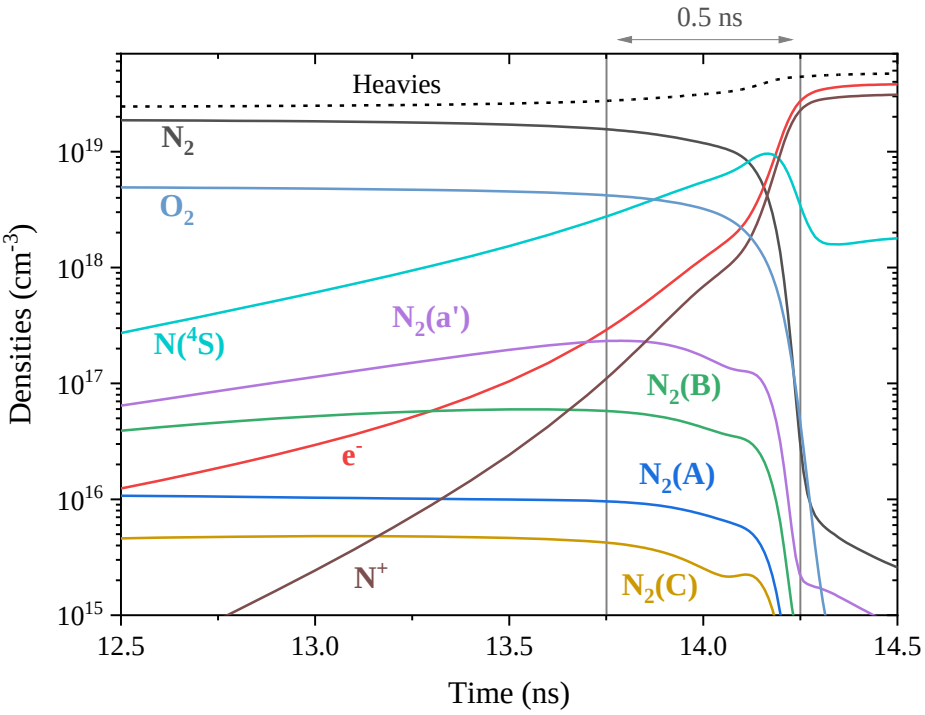

Fig. 4 Species density evolution during the generic 15-ns pulse of $E_0 = 47$ kV.cm^{-1} according to the 8-level model. The region of fast ionization is delimited by the grey lines between 13.75 and 14.25 ns. The total number density of heavy particles is also given (black dashed line).

Table 2 Plasma parameters before (t = 13.75 ns) and after (t = 14.25 ns) the fast ionization phase. At t = 14.25 ns, we calculate that 38% of atomic nitrogen is in the ground state ($3.5 \cdot 10^{18}$ cm^{-3}).

t (ns)	E/N (Td)	T_e (K)	T_{gas} (K)	N_2 (cm^{-3})	N (cm^{-3})	N^+ (cm^{-3})	n_e (cm^{-3})
13.75	172	34,400	2050	1.6×10^{19}	5.9×10^{18}	1.1×10^{17}	2.9×10^{17}
14.25	107	37,900	34,070	3.4×10^{15}	9.3×10^{18}	2.2×10^{19}	2.7×10^{19}

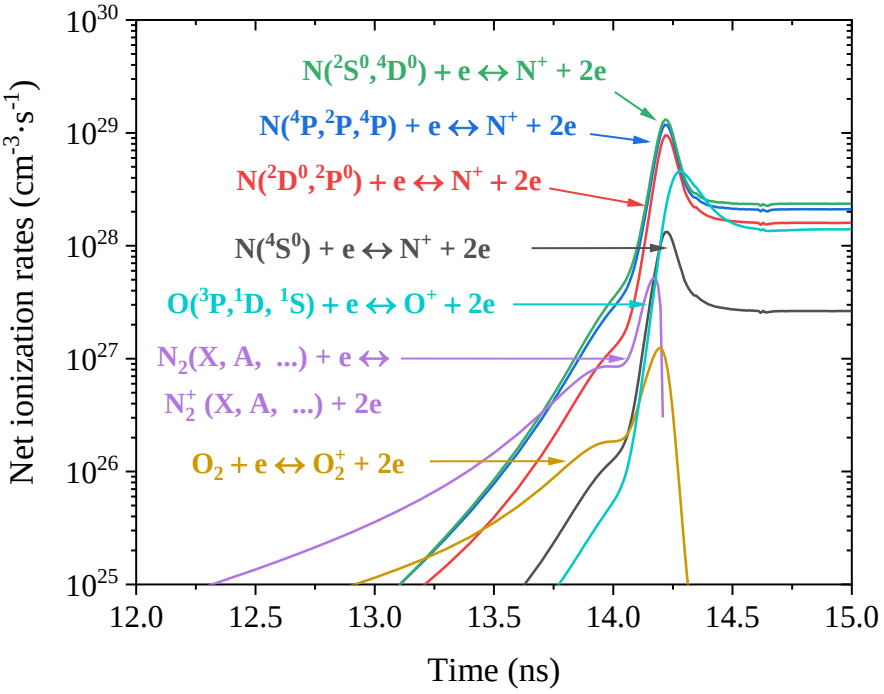

Fig. 5 Net electron production rate per unit volume. The net ionization rates of the two metastable states of N at 2.38 and 3.57 eV (in red) are added together. The next 5 levels are combined into two groups: E_i = 10.33, 10.68, 10.92 eV (in blue) and E_i = 11.60, 11.75 eV (in green). The net ionization rates of all N_2 and O electronic levels are also added (in purple and cyan, respectively).

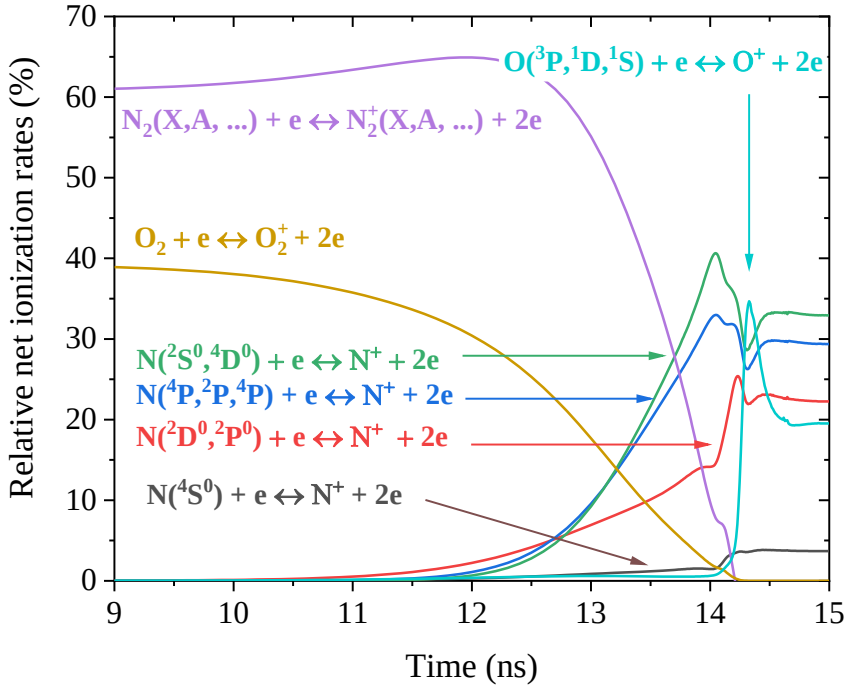

Fig. 6 Net ionization rates relative to the net electron production rate for the conditions of Fig. 5.

The origin of the fast ionization stage, shown in Fig. 3, and the impact of the ionization of N electronic states on the plasma kinetics are now discussed. In Fig. 5 and Fig. 6, the net rates[2] of the dominant ionization processes and their relative contributions are presented. The ionization rates of N_2 ground and excited states are summed for clarity and represented by a single curve. At $t < 10$ ns, the plasma is weakly ionized ($n_e < 10^{15}$ cm^{-3} according to Fig. 3) and the electron production is dominated by the ionization of N_2, N_2^*, and O_2. At $t = 12 - 13$ ns, the ionization of N excited states already represents ~ 10% of the total ionization, but the ionization of N(^{4}S) is still negligible. At $t = 13.75$ ns, the electrons are now mainly (~ 70 %) produced by electron-impact ionization of N excited states. Finally, at $t = 14.25$ ns, the peak of ionization is reached (> 10^{20} cm^{-3}·ns^{-1}) and the gas is already ionized above 50%. The N_2 and O_2 ionization rates rapidly decrease after $t = 14.2$ ns (Fig. 5) because the densities of N_2 and O_2 fall sharply at that instant (see Fig. 4). The contribution of O(^{3}P, ^{1}D, ^{1}S) ionization rates, shown in Fig. 6, reaches its maximum after the ionization peak. This delay, compared to N ionization, could be reduced if higher excited states of O were added to the kinetics.

Other ionization sources included in the initial kinetic mechanism of Flitti and Pancheshnyi are negligible [23]. For instance, using the rate of Guerra *et al.* [45], the associative ionization of N(^{2}D) and N(^{2}P), Reac. 5, is found to contribute to less than 0.04% in the electron and N_2^+ production.

$$N(^2D) + N(^2P) \rightarrow N_2^+ + e \qquad \text{Reac. 5}$$

Using the rate of Kossyi *et al.* [20], Reac. 6 is found to contribute at most 0.75% of the ionization at the peak of N_2(a') number density ($t = 14$ ns in Fig. 4).

$$N_2(a') + N_2(a') \rightarrow N_2^+ + N_2 + e \qquad \text{Reac. 6}$$

The electron-impact ionization of N_2(a'), initially not included in Ref. [23], is discussed in the Appendix.

[2] The recombination rate, computed by detailed balance, is subtracted from the ionization rate to give the "net electron production rate" or "net ionization rate" in cm^{-3}s^{-1}. This quantity has diverse denominations in the literature such as "reaction source term" or "chemical reaction flux".

V. Gas temperature increase

In typical non-equilibrium nanosecond spark discharges, the gas is weakly ionized ($n_e = 10^{15} – 10^{16}$ cm^{-3}) and the temperature of the heavy particles increases ($\Delta T \sim 1000$ K) mainly due to the ultrafast gas heating mechanism [4]. Models to determine the temperature evolution of non-equilibrium discharges are available in the literature [19,23,46,47]. In the present mechanism of thermal spark discharges, we incorporate only energy transfer through elastic and inelastic collisions between electrons and heavy particles (calculated by BOLSIG+). Gas heating associated with chemical reactions is neglected. We fixed the specific heat ratio to the classical value valid for monoatomic gases, *i.e.* $\gamma = 5/3 \approx 1.67$. We show in this section that, for thermal sparks, the typical T_{gas} increase due to the ultrafast gas heating mechanism is negligible compared to that of electron-ion elastic collisions.

In Fig. 7, when the plasma is weakly ionized ($t < 12$ ns), the electron temperature is constant around $T_e \sim 40{,}000$ K and the gas (or heavy) temperature remains equal to $T_{gas} = 300$ K. As the electron number density increases, the heavy particles and the electrons thermalize at $t \sim 14$ ns. The decrease of the reduced field (due to molecular dissociation) induces a global decrease of T_e during $t = 13.75 – 14.25$ ns. Near $t = 14$ ns, T_e increases and then decreases because the EEDF calculation depends on T_{gas} (see Eq. (27) in [24]). These variations vanish if we perform the simulation assuming $T_{gas} = 300$ K (not shown in the figure). Soon after, at $t = 15$ ns, the electrons are finally thermalized with the heavy particles at $T_{gas} = T_e = 37{,}000$ K.

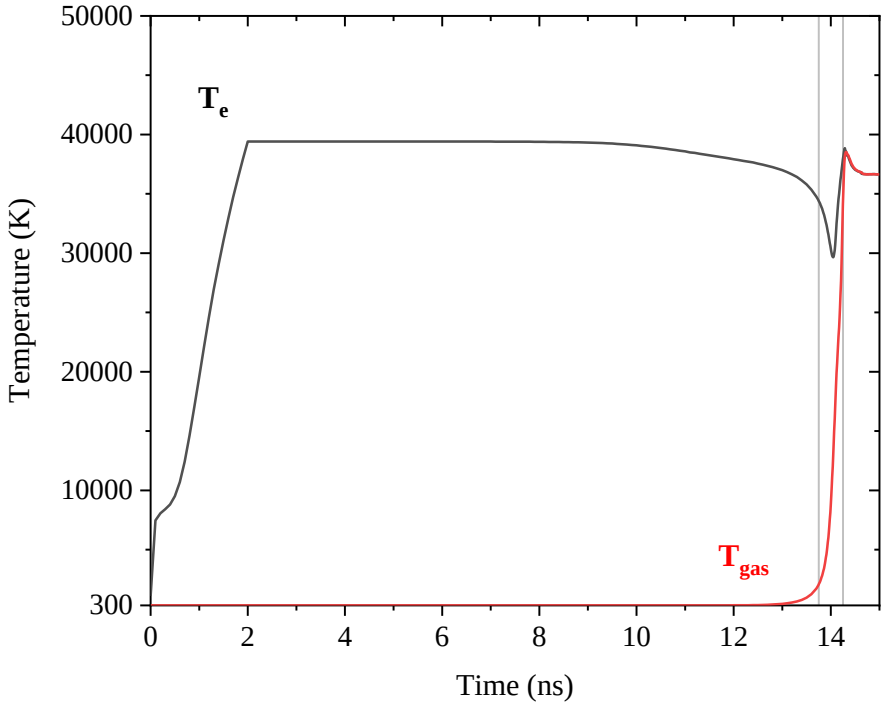

Fig. 7 Evolution of the electron and gas temperatures (in black and red, respectively). The fast increase of gas temperature occurs between the grey lines at 13.75 and 14.25 ns.

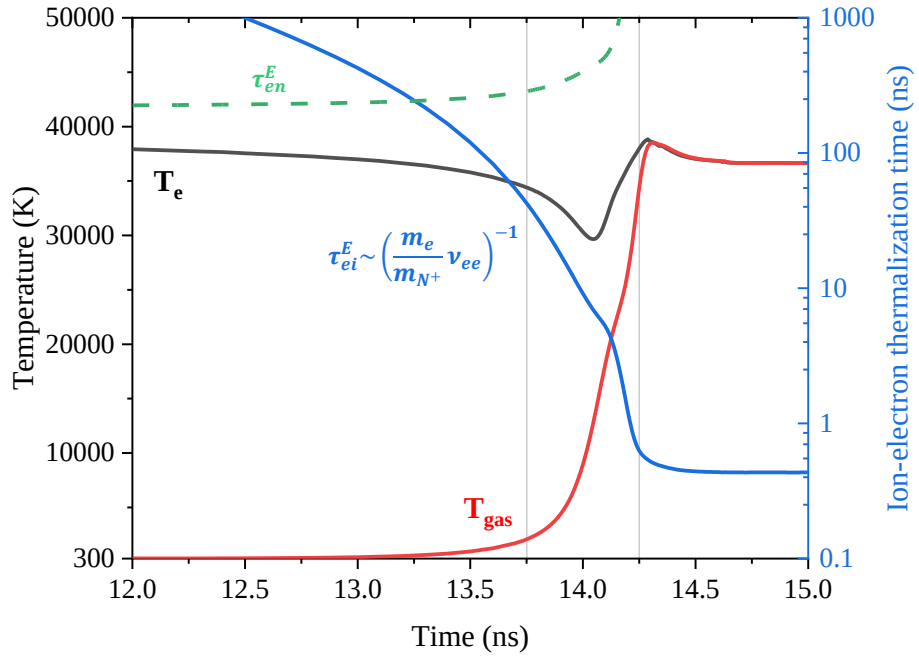

Fig. 8 Comparison of the temperature increase with the ion-electron thermalization time (in blue) for the conditions of Fig. 7. The electron-neutral thermalization time is provided for reference (dashed green).

We now provide first-order approximations of the electron-ion thermalization time. The electron-electron, ν_{ee}, and electron-ion, ν_{ei}, elastic collision frequencies can be estimated according to Eq. 3 where the mean thermal velocity of electrons is $v_e = \sqrt{8k_bT_e/\pi m_e} \sim 10^8$ cm·s^{-1}

$$\nu_{ei} \approx \nu_{ee} \approx n_e \sigma_{Coul} v_e \qquad \text{Eq. 3}$$

The cross-sections of elastic collisions between charged particles can be approximated by the Coulomb cross-section, σ_{Coul}, given in Eq. 4 where $\ln(\Lambda) = 13.57 + 1.5 \log(T_e) - 0.5 \log(n_e)$ [48].

$$\sigma_{Coul} \approx 2.87 \cdot 10^{-14} \frac{\ln(\Lambda)}{(T_e[\text{eV}])^2} [\text{cm}^2] \qquad \text{Eq. 4}$$

The formulation of Eq. 4 is a lower estimate of σ_{Coul} because the dependence on T_{gas} is neglected. Combining Eq. 3 and Eq. 4, we can calculate the characteristic time of energy exchange by elastic collisions, τ_{ei}^E in Eq. 5, which can also be seen as the ion-electron thermalization time.

$$\tau_{ei}^E \approx \left(\frac{m_e}{m_{N^+}} \nu_{ee}\right)^{-1} \qquad \text{Eq. 5}$$

Assuming the gas is mostly composed of N^+, the ratio of masses is m_{N^+}/m_e = 25,700. The evolution of τ_{ei}^E is given in Fig. 8. At t = 13.75 ns, $n_e \approx 10^{17}$ cm^{-3} and τ_{ei}^E decreases by two orders of magnitude until it reaches approximately 0.3 ns at t = 14.25 ns. At the same time, the gas temperature reaches 10,000 K in 0.25 ns, then 40,000 K in 0.5 ns. Once accelerated, ions can efficiently transfer their energy to the remaining neutral particles because their masses are similar. For comparison, the electron-neutral thermalization time, τ_{en}^E, remains above 200 ns and becomes much longer than τ_{ei}^E after t = 13.5 ns, as shown in Fig. 8. The thermalization by electron-ion collisions has already been discussed in the literature [40,49] and the critical electron number density was found to be around $n_e = 10^{16} – 10^{17}$ cm^{-3} [50,51], which is consistent with the present simulations.

VI. EEDF deviation from the Maxwellian distribution

As mentioned in Section III, the computation of the recombination rates relies on detailed balance, Eq. 2, valid only if the EEDF is Maxwellian. Also, the ionization rate constants of the highest excited states

of N (those with energies above 10 eV) were computed in Ref. [34] assuming a Maxwellian EEDF. In this section, we show that these approximations are valid when these processes are critical.

Departure from a Maxwellian distribution is expected in non-equilibrium plasmas generated by nanosecond discharges. The deviation δ(ε) from the Maxwellian distribution is defined in Eq. 6, where ε is the electron energy, $f(\varepsilon)$ the EEDF, and $f_M(\varepsilon)$ the corresponding Maxwellian distribution with the same mean energy as $f(\varepsilon)$.

$$\delta(\varepsilon) = \frac{f(\varepsilon)}{f_M(\varepsilon)} \qquad \text{Eq. 6}$$

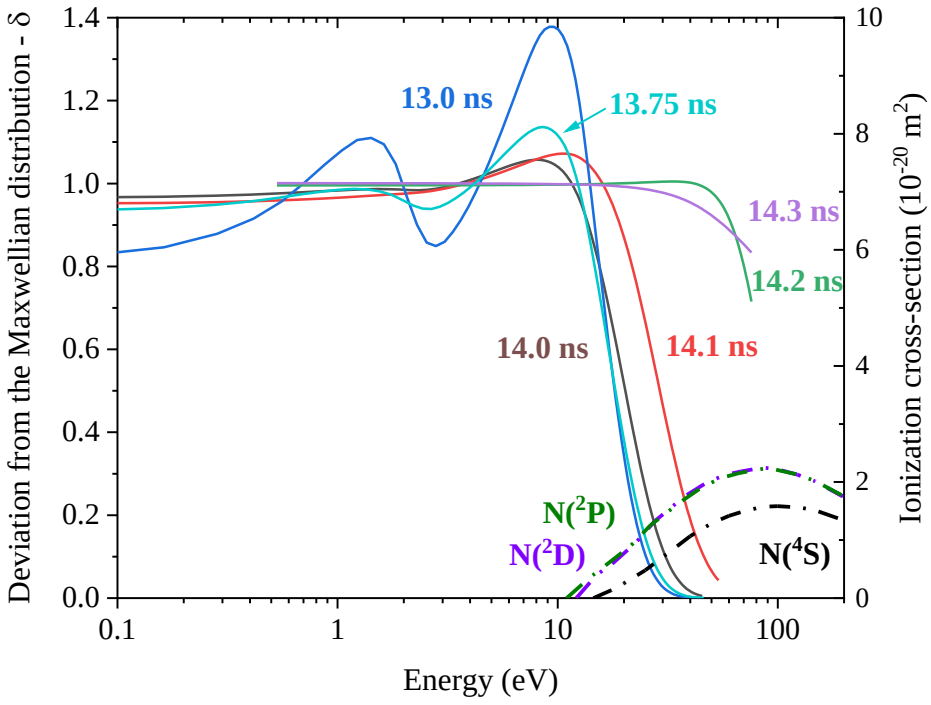

Fig. 9 Deviation (δ) of the EEDF from a Maxwellian EEDF of the same mean energy. The ionization cross-sections of N(^{4}S), N(^{2}D) and N(^{2}P) , taken from Ref. [32]**, are also shown for reference.**

A set of δ(ε) functions are shown in Fig. 9 for several instants. From t = 13.0 ns to t = 14.3 ns, the EEDF progressively thermalizes due to the high electron-electron collision frequency. At t = 14.3 ns, the electron number density is above 10^{19} cm^{-3} and the EEDF is very close to Maxwellian (i.e. δ(ε) ≈1).

The ionization rate coefficients of excited electronic states of N with energy above 10 eV (noted N**) are given by Arrhenius laws based on BEB cross-sections integrated with a Maxwellian EEDF in Ref. [34]. We now show that this approximation is valid when these rates are critical. The threshold of the N** ionization cross-sections lies at $\varepsilon \approx 3$ eV. In Fig. 9, we show that, in the 13 – 14.1 ns interval, $\delta(\varepsilon) = 1 \pm 0.4$ up to $\varepsilon = 25$ eV. The deviation from the corresponding Maxwellian EEDF is small and the ionization rates are approximately within a factor 1.4 from the Arrhenius rates. At later times, the EEDF rapidly becomes Maxwellian and its deviation is below 30% up to $\varepsilon = 100$ eV. The use of Arrhenius rates for N** ionization is therefore reasonable.

The recombination to excited electronic states becomes important only at $t > 14.2$ ns, as shown by the decay of the ionization rates in Fig. 5. After 14.2 ns, the EEDF approaches a Maxwellian. It is, therefore, valid to use detailed balance for recombination rate calculations at these times.

VII. Influence of the number of atomic states

The atomic nitrogen excited electronic states play a significant role in electron production. New simulations are performed, changing the number of N and O atomic excited states included in the kinetic mechanism. The initial reduced field is equal to $(E/N)_0 = 195$ Td in ambient conditions and given by Eq. 1. The evolution of the electron number density is shown in Fig. 10. The 8-level model, represented in Fig. 2 and studied in previous sections, will be the reference for comparison. Simulations with only the first six excited states of nitrogen ($E_{up} < 11.61$ eV in Table 1) lead to similar results as in previous sections: the fast ionization stage now lasts 0.75 ns (instead of 0.5 ns). However, if only the first three levels of nitrogen are included, full ionization is not reached by the end of the 15-ns pulse. If the field were applied for a longer duration, full ionization would be reached, but without an abrupt increase. An intermediate result is obtained by including four or five levels.

Finally, only including the ionization of $N(^4S)$ and $O(^3P)$, *i.e.* the ground states, decreases the maximal electron number density by two orders of magnitude compared to the 8-level model. Note that the ionization of N_2 excited states is always included. The deviation between the models starts at

t = 12.5 – 13.0 ns, corresponding to $n_e = 10^{16} – 10^{17}$ cm^{-3}. We therefore conclude that if $n_e \geq 10^{16}$ cm^{-3}, the correct description of the plasma kinetics must include at least the first six electronic states of N and the first three electronic states of O.

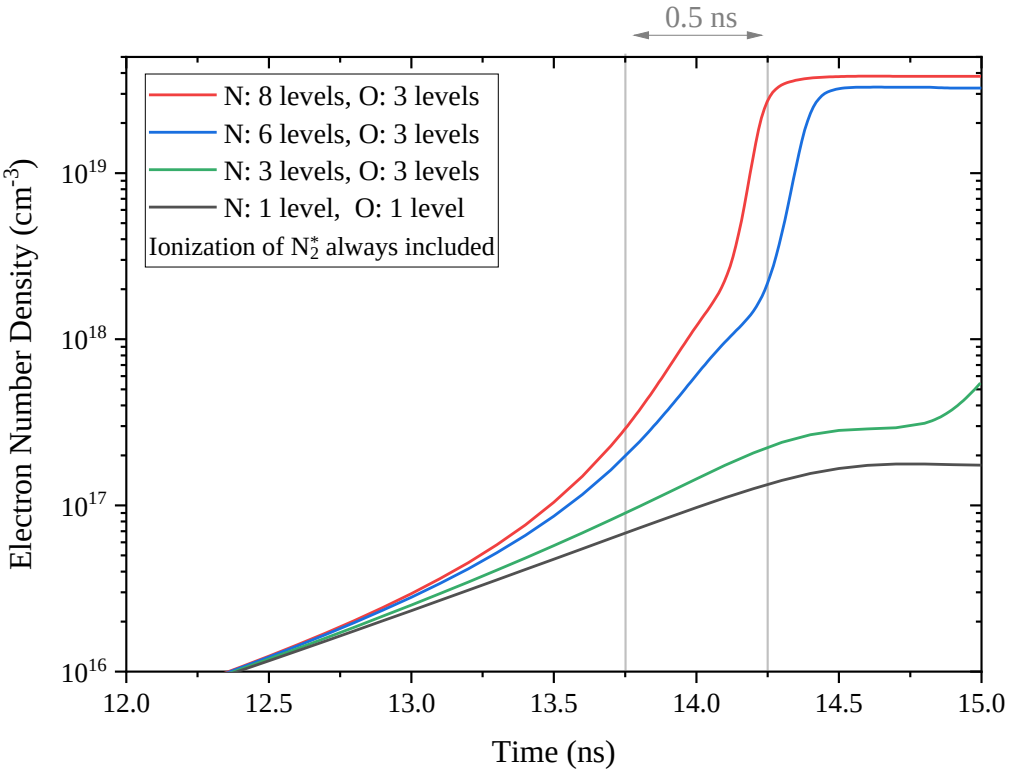

Fig. 10 Temporal evolution of n_e for simulations including three, six, and eight electronic states of N (in green, blue, and red respectively) and three electronic states of O. The n_e evolution computed considering only N(^{4}S) and O(^{3}P) is also shown (in grey). The region of fast ionization of the 8-level model is delimited by the grey lines at 13.75 and 14.25 ns.

Qualitatively, the model of Ref. [16] corresponds to the grey curve in Fig. 10. In Ref. [16], the ionization of N_2 electronic excited states was claimed to be responsible for the full ionization of the gas (nanosecond SDBD in pure N_2 at 5 atm), which seems to be in disagreement with our present conclusions. Indeed, by the time the simulation is stopped in Ref. [16], the ionization reaches ~ 1%, which corresponds to the moment atomic excited states ionization dominates. Also in Ref. [16], the heat released by the recombination of N_2^+ and O_2^+ was stated to be responsible for gas thermalization in their conditions, which is not in agreement with our findings. Although N_2^+ and O_2^+ recombination could have an impact, the heating due to electron-ion collisions is sufficient to explain the increase of temperature in the present simulations (see Fig. 8).

VIII. Comparison with an early Maxwellian EEDF

To our knowledge, BOLSIG+ was tested up to an ionization fraction of 1% [25]. Also, we assumed in Section II that N is the total heavy particle density in the E/N formulation, i.e. $N = N_{ions} + N_{neutrals}$. It is worth noting that for $n_e < 10^{18}$ cm^{-3}, this formulation does not influence the results of the present work. For $n_e > 10^{18}$ cm^{-3}, we performed a simulation referred to as "early Maxwellian EEDF". The initial conditions of the early Maxwellian EEDF simulation are taken at $t = 13.75$ ns (see Table 2). In this specific simulation and only for $t > 13.75$ ns, the EEDF is Maxwellian with $T_e = 34{,}400$ K. The variations of n_e and T_e in the early Maxwellian EEDF model are compared with the 8-level model in Fig. 11. The same fast increase of n_e is observed with the early Maxwellian EEDF (2 decades increase in 0.5 ns). Comparable results are also obtained if T_e is set to 37,900 K (see Table 2) instead of 34,400 K in the early Maxwellian EEDF simulation.

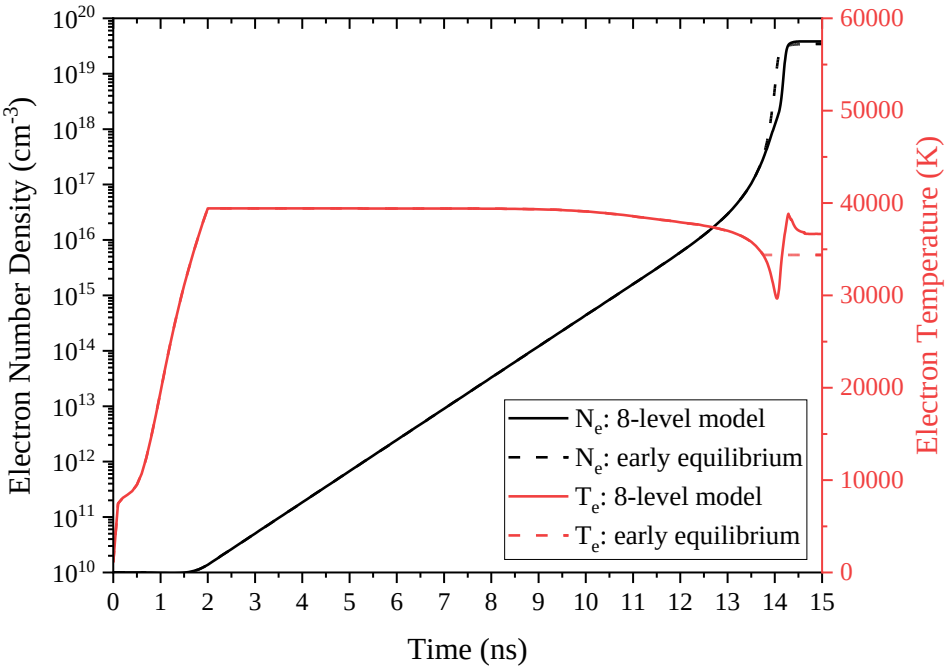

Fig. 11 Comparison of the electron number density (in black) and electron temperature (in red) evolution with the early Maxwellian equilibrium. The solid and dashed lines represent the results of the 8-level model and the early Maxwellian EEDF model, respectively.

Thus, the plasma kinetics could have been computed assuming $T_e = 35{,}000 – 40{,}000$ K during the entire simulation. However, the use of E/N allows for a comparison with the experimental electron

temperatures obtained in the literature. Indeed, the temperatures we obtain here are close to what was experimentally measured by a fit of N^+ lines in previous works [7,13]. A temperature of T_e = 39,000 ± 4000 K was obtained in the early afterglow of a 10-ns discharge of 8-kV applied between pins separated by 3 mm [13], and T_e = 45,000 ± 5000 K was measured in a 2-mm discharge after a 5.5-kV pulse [7]. In a pin-to-pin configuration, Orriere *et al.* [12] measured an electron temperature of 72,000 ± 10,000 K and 37,000 ± 4,000 K at t = 15 ns and t = 30 ns, respectively, during a 2.5-kV discharge across a 200-μm gap. A longer duration discharge was applied by Lo *et al.* [11] across a gap of 3 mm, and a temperature ranging from 30,000 K to 45,000 K was measured. Also, in the early phase (t < 30 ns) of a spark-plug discharge of 3 kV in a 1-mm gap, Albrecht *et al.* [52] measured an electron temperature ranging between 60,000 and 30,000 K. All the experiments mentioned above reached full ionization within a few nanoseconds. A more exhaustive comparison between these experiments is given in Ref. [7]. Therefore, we conclude that the temperature obtained (in the 8-level model) or imposed (in the early Maxwellian model) in Fig. 11 adequately represents the experiments reported above.

We also checked, using the ionization cross-sections of Tawara and Kato [35], that doubly ionized ions, N^{++} and O^{++}, play a negligible role. We obtained that the maximal density of N^{++} is approximately 10^{18} cm^{-3} at the end of the pulse. This result agrees with the work of Sher *et al.*, who calculated the plasma composition after isochoric heating between 40,000 K – 45,000 K [Fig. 2, 53] and with experimental findings, where the N^{++} lines were not detected [7,10–13].

Finally, it could be argued that BOLSIG+ calculates quasi-stationary solutions of the Boltzmann equation, which is not compatible with the abrupt variations of the plasma composition. The typical time to form the stationary EEDF is about 10 ps in similar conditions (see "case study 3" in Ref. [54]) while we used a 2-ps time step. However, at t > 13.75 ns, the quasi-stationary approximation has a minor effect thanks to the two following points:

- For t > 13.75 ns, the electron number density is above 10^{17} cm^{-3} (see Table 2). Thus, the EEDF is close to a Maxwellian because of the electron-electron collisions (see Section VI).
- We showed in this section that the abrupt full ionization is only weakly dependent on the EEDF shape.

Therefore, in the present conditions, the time-dependent solution of the Boltzmann equation would provide similar results in terms of kinetics. It would be interesting for future work to implement time-dependent calculations of the EEDF and quantify this effect for partially ionized plasmas.

Conclusions

The mechanism of ionization in ambient air by a 15-ns pulse of 47 $kV \cdot cm^{-1}$ was studied with 0-D simulations using ZDPlaskin and BOLSIG+. The electron production phase is first dominated by electron-impact ionization of N_2 and O_2. Then, molecules dissociate, and the density of atomic species increases. Excited electronic states of atoms and molecules are populated by electron-impact excitation. For $n_e > 10^{16}$ cm^{-3}, the simulations reveal that the ionization of N excited states dominates over the ionization of N_2(X, A, B, a', C). The electron number density increases by two orders of magnitude (from 10^{17} cm^{-3} to more than 10^{19} cm^{-3}) in less than half a nanosecond. Neglecting the ionization of the electronic excited states of O and N fails to reproduce this behavior. Simultaneously, the gas temperature increases from 300 to 37,000 K due to electron-ion elastic collisions. The EEDF is found to be Maxwellian by the time the plasma is fully ionized. This mechanism explains, in our opinion, the fast transition (< 1 ns) from a non-equilibrium to a thermal plasma, as experimentally observed with nanosecond discharges in Refs. [7–13].

Acknowledgments

This work has been supported by the French National Research Agency (ANR-16-CE22-0005 PASTEC ANR-16-CE30-0004 ASPEN). N. Minesi has been supported by an IDEX Ph.D. fellowship (ANR-11-IDEX-0003-02). The authors would like to thank Dr. Sergey Pancheshnyi for his advice on ZDPlasKin, Dr. Nikolay Popov and Dr. Gerjan Hagelaar for helpful discussions about this work. The authors also express their gratitude to all the contributors of LXCat, BOLSIG+, and ZDPlasKin.

Appendix

In most figures, the transition between a non-equilibrium to a thermal plasma is marked by the two grey lines at 13.75 and 14.25 ns. By the end of this transition, the ground and excited states of N_2 are

completely dissociated. The evolution of N_2(a'), in Fig. 4, is surprisingly peaked compared to the other excited states. This is explained by differences in the dissociation cross-sections shown in Fig. 12. As the energy of the electrons increases, it is expected that the N_2 excited states dissociate before they ionize, except N_2(a') which has a much lower dissociation cross-section. This is confirmed in Fig. 13, where the net ionization rates of N_2 electronic states to N_2^+(X, A, B, C) are plotted against time. For t > 13 ns, the ionization rate of N_2(a') is higher than the ionization rate N_2(X).

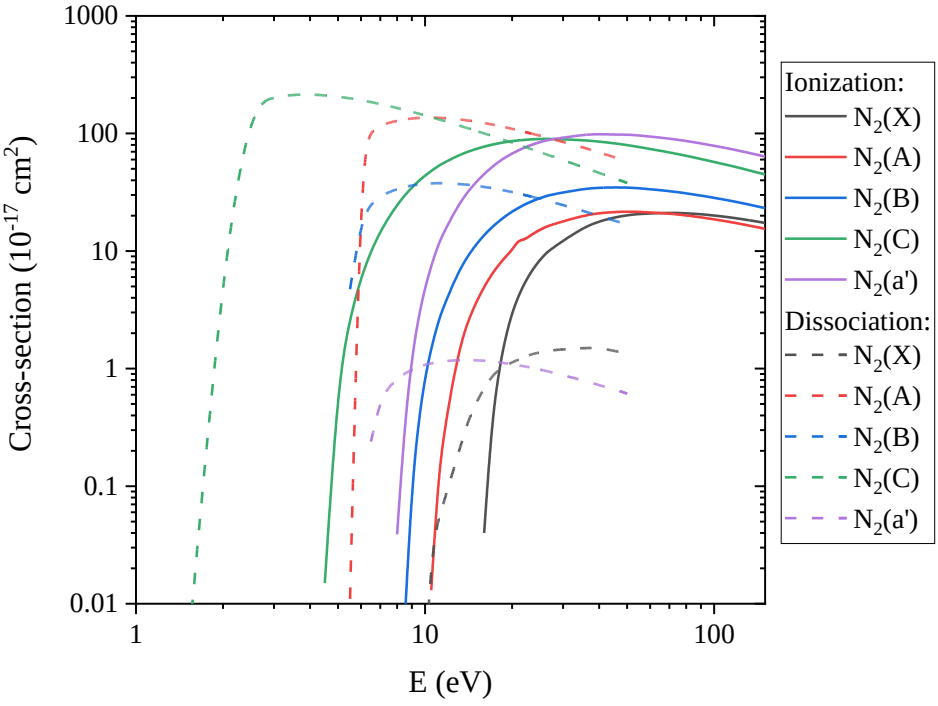

Fig. 12 Ionization and dissociation cross-sections by electron impact [31]**. The dissociation cross-section of N_2(a') is much lower than those of other excited states, whereas its ionization cross-section is comparable.**

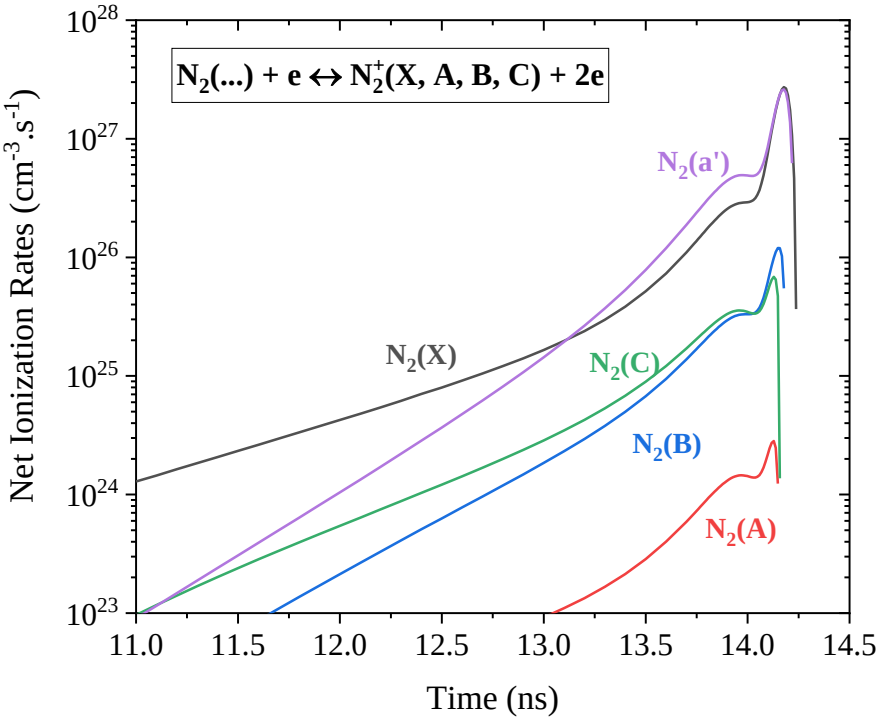

Fig. 13 Net ionization rates per unit of volume of N_2(A, B, C, a') (in red, blue, green, and purple) compared with the ground state (in grey). The curves stop at the point where recombination becomes higher than ionization.

References

[1] Pai D Z, Stancu G D, Lacoste D A and Laux C O 2009 Nanosecond repetitively pulsed discharges in air at atmospheric pressure - The glow regime *Plasma Sources Sci. Technol.* **18** 045030

[2] Pai D Z, Lacoste D A and Laux C O 2010 Transitions between corona, glow, and spark regimes of nanosecond repetitively pulsed discharges in air at atmospheric pressure *J. Appl. Phys.* **107** 093303

[3] Pai D Z, Lacoste D A and Laux C O 2010 Nanosecond repetitively pulsed discharges in air at atmospheric pressure-the spark regime *Plasma Sources Sci. Technol.* **19** 065015

[4] Rusterholtz D L, Lacoste D A, Stancu G D, Pai D Z and Laux C O 2013 Ultrafast heating and oxygen dissociation in atmospheric pressure air by nanosecond repetitively pulsed discharges *J. Phys. D. Appl. Phys.* **46** 464010

[5] Brisset A, Gazeli K, Magne L, Pasquiers S, Jeanney P, Marode E and Tardiveau P 2019 Modification of the electric field distribution in a diffuse streamer-induced discharge under extreme overvoltage *Plasma Sources Sci. Technol.* **28** 055016

[6] Lepikhin N D, Klochko A V., Popov N A and Starikovskaia S M 2016 Long-lived plasma and fast quenching of N2(C3Π u) by electrons in the afterglow of a nanosecond capillary discharge in nitrogen *Plasma Sources Sci. Technol.* **25** 045003

[7] Minesi N, Stepanyan S, Mariotto P, Stancu G D and Laux C O 2020 Fully ionized nanosecond discharges in air: the thermal spark *Plasma Sources Sci. Technol.* **29** 85003

[8] Parkevich E V., Medvedev M A, Khirianova A I, Ivanenkov G V., Agafonov A V., Selyukov

A S, Mingaleev A R, Shelkovenko T A and Pikuz S A 2019 Investigation of a Near-Electrode Plasma Formed in the Atmospheric Discharge with Employment of Picosecond Laser Probing *J. Russ. Laser Res.* **arXiv:1804**

[9] Parkevich E V., Khirianova A I, Agavonov A V., Tkachenko S I, Mingaleev A R, Shelkovenko T A, Oginov A V. and Pikuz S A 2018 Anode Plasma Formation at the Initial Stage of a Nanosecond Air Discharge *J. Exp. Theor. Phys.* **126** 422–9

[10] van der Horst R M, Verreycken T, van Veldhuizen E M and Bruggeman P J 2012 Time-resolved optical emission spectroscopy of nanosecond pulsed discharges in atmospheric-pressure N 2 and N 2 /H 2 O mixtures *J. Phys. D. Appl. Phys.* **45** 345201

[11] Lo A, Cessou A, Lacour C, Lecordier B, Boubert P, Xu D A, Laux C O and Vervisch P 2017 Streamer-to-spark transition initiated by a nanosecond overvoltage pulsed discharge in air *Plasma Sources Sci. Technol.* **26** 45012

[12] Orriere T, Moreau E and Pai D Z 2018 Ionization and recombination in nanosecond repetitively pulsed microplasmas in air at atmospheric pressure *J. Phys. D. Appl. Phys.* **51** 494002

[13] Minesi N, Stepanyan S A, Mariotto P B, Stancu G-D and Laux C O 2019 On the arc transition mechanism in nanosecond air discharges *AIAA Scitech 2019 Forum* **2019** 0463

[14] Sainct F P, Urabe K, Pannier E, Lacoste D A and Laux C O 2020 Electron number density measurements in nanosecond repetitively pulsed discharges in water vapor at atmospheric pressure *Plasma Sources Sci. Technol.* **29** 025017

[15] Shcherbanev S A, Yu Khomenko A, Stepanyan S A, Popov N A and Starikovskaia S M 2016 Optical emission spectrum of filamentary nanosecond surface dielectric barrier discharge *Plasma Sources Sci. Technol.* **26** 02LT01

[16] Shcherbanev S A, Ding C, Starikovskaia S M and Popov N A 2019 Filamentary nanosecond surface dielectric barrier discharge. Plasma properties in the filaments *Plasma Sources Sci. Technol.* **28** 065013

[17] Stepanyan S A, Starikovskiy A Y, Popov N A and Starikovskaia S M 2014 A nanosecond surface dielectric barrier discharge in air at high pressures and different polarities of applied pulses: transition to filamentary mode *Plasma Sources Sci. Technol.* **23** 045003

[18] Macheret S O, Shneider M N and Miles R B 2002 Modeling of air plasma generation by repetitive high-voltage nanosecond pulses *IEEE Trans. Plasma Sci.* **30** 1301–14

[19] Popov N A 2016 Kinetics of plasma-assisted combustion: effect of non-equilibrium excitation on the ignition and oxidation of combustible mixtures *Plasma Sources Sci. Technol.* **25** 043002

[20] Kossyi I A, Kostinsky A Y, Matveyev A A and Silakov V P 1992 Kinetic scheme of the non-equilibrium discharge in nitrogen-oxygen mixtures *Plasma Sources Sci. Technol.* **1** 207–20

[21] Capitelli M, Ferreira C M, Gordiets B F and Osipov A I 2000 *Plasma Kinetics in Atmospheric Gases* vol 31 (Berlin, Heidelberg: Springer Berlin Heidelberg)

[22] Pancheshnyi S V, Eismann B, Hagelaar G J M and Pitchford L C 2008 Computer code ZDPlasKin

[23] Flitti A and Pancheshnyi S 2009 Gas heating in fast pulsed discharges in N 2 –O 2 mixtures *Eur. Phys. J. Appl. Phys.* **45** 21001

[24] Hagelaar G J M and Pitchford L C 2005 Solving the Boltzmann equation to obtain electron transport coefficients and rate coefficients for fluid models *Plasma Sources Sci. Technol.* **14** 722–33

[25] Hagelaar G J M 2016 Coulomb collisions in the Boltzmann equation for electrons in low-

temperature gas discharge plasmas *Plasma Sources Sci. Technol.* **25** 015015

[26] www.lxcat.net, retrieved on April 4 2019. *BSR database*

[27] www.lxcat.net, retrieved on March 1 2019 *IST-Lisbon database*

[28] www.lxcat.net, retrieved on March 1 2019 *Hayashi database*

[29] www.lxcat.net, retrieved on March 1 2019 *Morgan Database*

[30] Pancheshnyi S V 2020 _ *Pers. Commun.*

[31] Bacri J and Medani A 1982 Electron diatomic molecule weighted total cross section calculation. III. Main inelastic processes for N2 and N2+ *Phys. B+C* **112** 101–18

[32] Wang Y, Zatsarinny O and Bartschat K 2014 B-spline R-matrix-with-pseudostates calculations for electron-impact excitation and ionization of nitrogen *Phys. Rev. A* **89** 062714

[33] Tayal S S and Zatsarinny O 2016 B -spline R -matrix-with-pseudostates approach for excitation and ionization of atomic oxygen by electron collisions *Phys. Rev. A* **94** 1–15

[34] Ciccarino C J and Savin D W 2019 Electron-impact ionization of atomic nitrogen *J. Thermophys. Heat Transf.* **33** 154–62

[35] Tawara H and Kato T 1987 Total and partial ionization cross sections of atoms and ions by electron impact *At. Data Nucl. Data Tables* **36** 167–353

[36] Biberman L M, Vorob'Ev V S and Yakubov I T 1973 Kinetics of impact-radiation ionization and recombination *Sov. Phys. - Uspekhi* **15** 375–94

[37] Bourdon A and Vervisch P 1996 Three-body recombination rate of atomic nitrogen in low-pressure plasma flows *Phys. Rev. E - Stat. Physics, Plasmas, Fluids, Relat. Interdiscip. Top.* **54** 1888–98

[38] Park C 1973 Comparison of electron and electronic temperatures in recombining nozzle flow of ionized nitrogen-hydrogen mixture. part 2. experiment *J. Plasma Phys.* **9** 217–34

[39] Annaloro J, Morel V, Bultel A and Omaly P 2012 Global rate coefficients for ionization and recombination of carbon, nitrogen, oxygen, and argon *Phys. Plasmas* **19** 073515

[40] Almazova K I, Belonogov A N, Borovkov V V, Khalikova Z R, Ragimkhanov G B, Tereshonok D and Trenkin A A 2020 Investigation of plasma properties in the phase of the radial expansion of spark channel in the pin-to-plate geometry *Plasma Sources Sci. Technol.*

[41] Lopez B, Johnston C O and Panesi M 2016 Improved non-boltzmann modeling for nitrogen atoms *46th AIAA Thermophys. Conf.* 13–7

[42] Biberman L M, Vorob'ev V S, Yakubov I T and Cecchi J L 1989 Kinetics of Nonequilibrium Low-Temperature Plasmas *Phys. Today* **42** 65–6

[43] Alberty R A and Silbey R J 1992 *Physical chemistry 1st Edition* (John Wiley & Sons, Inc.)

[44] Dresvin S V. 1977 *Physics and technology of low-temperature plasmas* (Press, The Iowa State University)

[45] Guerra V, Sá P A and Loureiro J 2004 Kinetic modeling of low-pressure nitrogen discharges and post-discharges *EPJ Appl. Phys.* **28** 125–52

[46] Bak M S and Cappelli M A 2015 A reduced set of air plasma reactions for nanosecond pulsed plasmas *IEEE Trans. Plasma Sci.* **43** 995–1001

[47] Aleksandrov N L, Kindysheva S V, Nudnova M M and Starikovskiy A Y 2010 Mechanism of ultra-fast heating in a non-equilibrium weakly ionized air discharge plasma in high electric fields

J. Phys. D. Appl. Phys. **43** 255201

[48] Raizer Y P 1991 *Gas Discharge Physics* ed J E Allen (Springer Verlag. Berlin.)

[49] Bastien F and Marode E 1979 The determination of basic quantities during glow-to-arc transition in a positive point-to-plane discharge *J. Phys. D. Appl. Phys.* **12** 249–63

[50] Stritzke P, Sander I and Raether H 1977 Spatial and temporal spectroscopy of a streamer discharge in nitrogen *J. Phys. D. Appl. Phys.* **10** 2285–300

[51] Barreto E, Jurenka H and Reynolds S I 1977 The formation of small sparks *J. Appl. Phys.* **48** 4510–20

[52] Albrecht H, Bloss W H, Herden W H, Maly R, Saggau B and Wagner E 1977 New Aspects on Spark Ignition *SAE Tech. Pap.* 770853

[53] Sher E, Ben-Ya'ish J and Kravchik T 1992 On the birth of spark channels *Combust. Flame* **89** 186–94

[54] Capitelli M, Colonna G, D'Ammando G and Pietanza L D 2017 Self-consistent time dependent vibrational and free electron kinetics for CO2 dissociation and ionization in cold plasmas *Plasma Sources Sci. Technol.* **26**